JUSTC

Article

http://justc.ustc.edu.cn

Received: April 22, 2025; Accepted: June 07, 2025

Bacterial surface behavior revealed using simple digital holographic microscopy

Xinyi Feng, and Rui He ✉

Department of Physics, University of Science and Technology of China, Hefei 230026, China

✉Correspondence: Rui He, E-mail: ruihe@ustc.edu.cn

Graphical abstract

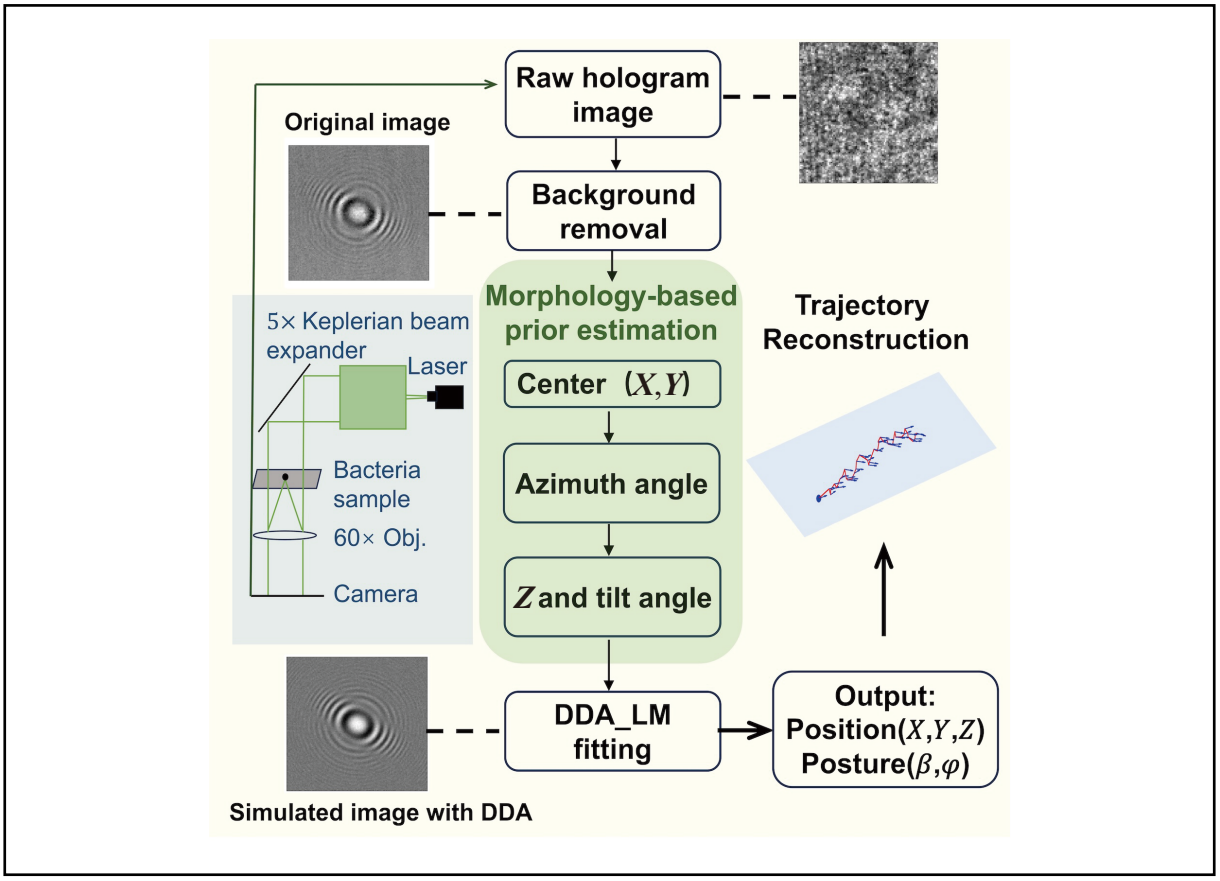

Workflow of digital holographic microscopy for quantitative 3D tracking of bacterial position and posture near surfaces.

Public summary

- A simple digital holographic microscopy (DHM) system enables high-throughput, label-free imaging of *E. coli* swimming near surfaces.
- A robust workflow combining background correction, morphology-based prior estimation, and DDA-LM fitting achieves quantitative 3D tracking of bacterial position and orientation.
- Our method reveals dynamic swimming parameters, including trajectory geometry, body tilt, and wobble, with high spatial and temporal resolution.

Citation: Feng X Y, He R. Bacterial surface behavior revealed using simple digital holographic microscopy. *JUSTC*, **2025**, 55(10): 1003. CSTR: 32290.14.JUSTC-2025-0050. DOI: 10.52396/JUSTC-2025-0050

JUSTC

Article

http://justc.ustc.edu.cn

Received: April 22, 2025; Accepted: June 07, 2025

Bacterial surface behavior revealed using simple digital holographic microscopy

Xinyi Feng, and Rui He ✉

Department of Physics, University of Science and Technology of China, Hefei 230026, China

✉Correspondence: Rui He, E-mail: ruihe@ustc.edu.cn

Cite This: *JUSTC*, **2025**, 55(10): 1003 (10pp)

Read Online

SI Supporting Information

Abstract: Flagellated bacteria exhibit significantly altered motility near solid–liquid interfaces, affecting key biological processes such as biofilm formation and pathogenic infection. In this study, we present a simplified in-line digital holographic microscopy (DHM) system tailored for high-throughput, label-free imaging of *Escherichia coli* (*E. coli*) swimming in near-surface environments. By applying a sliding median filter and mean normalization, we effectively suppress speckle noise and background artifacts in holograms. We introduce a morphology-aware workflow combining a voting algorithm, fast Fourier transform (FFT) analysis, and Bayesian optimization to robustly estimate bacterial positions and orientations, overcoming instability challenges common in non-spherical scattering models. Additionally, we employ a discrete dipole approximation (DDA) with a Levenberg–Marquardt (LM) optimizer to simulate and fit holographic interference patterns, achieving submicron axial precision and accurate tilt and azimuth angle measurements near surfaces. Through experiments tracking *E. coli* near surfaces, we quantitatively characterize swimming speed, trajectory geometry, and cell body orientation with high temporal resolution, revealing critical features of near-surface bacterial motility. Our results demonstrate the feasibility of single-beam DHM for rapid, quantitative tracking of bacterial surface behavior, providing an accessible and powerful tool for investigating microbe—interface interactions in biophysical and biomedical research.

Keywords: digital holographic microscopy; bacterial surface motility; *Escherichia coli* tracking

CLC number: Q6-3 **Document code:** A

1 Introduction

In both natural and biomanufacturing environments, microorganisms frequently encounter solid–liquid interfaces. For flagellated bacteria such as *Escherichia coli* (*E. coli*), motility near surfaces can differ markedly from that in bulk liquid environments[1–3]. Previous studies have shown that when bacteria approach a surface, their swimming speed, tumble frequency, body tilt angle, and flagellar wobble dynamics can all undergo notable changes[4,5]. These modifications are closely linked to bacterial adhesion, biofilm formation, and pathogenic infection processes. However, accurately capturing the three-dimensional position and posture of bacteria in real time remains challenging, as traditional microscopic methods are often limited by field of view and depth resolution[6], making it difficult to balance high temporal resolution with a large depth of field.

In recent years, digital holographic microscopy (DHM) has rapidly emerged as a powerful tool for studying microbial movement[7–13]. Its core principle is to use coherent light fields to capture amplitude and phase information of the target by recording interference fringes, enabling the three-dimensional distribution of the target to be obtained through numerical reconstruction or physical modeling[7]. Compared to ordinary microscopes, DHM offers several advantages: It is label-free, high-throughput, capable of fast real-time imaging, and provides a large depth of field[14,15]. It does not require fluorescent labeling or staining, and a single exposure can capture a hologram containing three-dimensional information. Modern CMOS/CCD cameras can achieve hundreds to thousands of frames per second, making DHM suitable for imaging rapidly swimming bacteria. Additionally, it allows numerical reconstruction of any focal plane during post-processing[16], thereby avoiding the time delay associated with mechanical focusing.

However, existing digital holographic research on the three-dimensional motion of microorganisms faces several technical limitations. On the one hand, traditional numerical reconstruction methods lack precision for weakly scattering or non-spherical rod-shaped bacteria[17]. On the other hand, holographic fitting methods based on physical models, such as Mie scattering and the discrete dipole approximation (DDA), are often sensitive to initial parameters and require substantial computational resources to ensure convergence[5,18]. Although Bianchi et al.[5] captured the inclination angle of bacteria adhering to surfaces using holographic technology, their three-beam optical system is complex, and the cumbersome experimental setup limits the generalizability of the tracking method. Wang et al.[18] tracked the motion of *E. coli* in free liquid using a single light source, but their method still

CSTR: 32290.14.JUSTC-2025-0050
DOI: 10.52396/JUSTC-2025-0050
JUSTC, **2025**, 55(10): 1003

needs improvements in fitting time and accuracy. To address these shortcomings, this paper proposes using a physical scattering model—DDA combined with numerically optimized initial parameter estimation via the Levenberg–Marquardt (LM) algorithm to fit holographic images, thereby enabling tracking of bacterial near-surface motion.

In practical experiments with DHM, annoying patterns often appear due to dirty spots in the light path or lens defects. To obtain analyzable images, background correction techniques are essential. Here, we simply applied a sliding median filter and mean normalization to preprocess the original images. Surprisingly, this approach effectively removes transient signals and smooths light intensity drift, while enhancing the contrast of interference fringes of bacteria.

The key to implementing 3D tracking with the DHM technique is the algorithm to extract the position (X, Y, Z) and posture (inclination angle β and azimuth angle φ) of bacteria from the fringes they generated. Here, we designed an automatic initial parameter estimation method to extract these five parameters. First, by combining a voting method with fast Fourier transform (FFT) analysis, we rapidly and accurately localized the bacterial center position (X, Y) and azimuth angle (φ), avoiding the efficiency and accuracy losses typical of traditional methods, like Hough transformation, when dealing with non-circular targets. Next, based on morphological priors of the typical geometric size of *E. coli*, we generated interference patterns with varying inclination angles around the Z position estimated from the fringes in the original images. Subsequently, the bacterial axial position (Z) and inclination angle (β) were obtained through joint Bayesian optimization. These operations provide a more precise initialization for fitting the three-dimensional position and posture of bacteria.

The algorithm maintains globally stable convergence even when bacteria undergo significant angular or positional changes near the surface and greatly improves the processing efficiency of the LM algorithm. Using this approach, high-precision measurements of bacterial three-dimensional position and posture can be obtained under single-beam optical experimental conditions. To validate the feasibility of the algorithm, we conducted experiments with *E. coli*, and with the algorithm we successfully captured key dynamic parameters of swimming bacteria, including movement speed, trajectory morphology, and wobble frequency.

2 Materials and methods

2.1 Bacterial culturing

We used wild-type *E. coli* (strain HCB1) to perform the tracking experiment. The cells were cultured in LB broth (Lysogeny Broth, composed of 1%(w/v) Bacto™ Tryptone (Gibco), 0.5%(w/v) yeast extract, and 0.5%(w/v) sodium chloride) with shaking at 33 °C and 200 r/min overnight. Subsequently, 100 μL of overnight solution was added to 10 mL of TB broth (similar to LB but without yeast extract) and harvested at OD of 0.5. The cells were diluted 1:10 with motility medium (10 mM potassium phosphate, 0.1 mM ethylenediaminetetraacetic acid, 1 μM L-methionine, 10 mM lactic acid, pH 7.0).

2.2 Sample preparation

Chambers were created by attaching an 18 mm × 18 mm coverslip on a 24 mm × 60 mm coverslip with ~70 μm thick double-sided tapes. Each coverslip was cleaned with ultrasonic cleaner in dH_2O and alcohol for five times. About 40 μL of bacterial suspension was injected into the chamber and sealed with Apiezon vacuum grease.

2.3 Optical path and holographic image acquisition

The optical path of the online holographic system is shown in Fig. 1. A 532 nm solid-state laser (MGL-III-532-100mW) coupled with a fiber was used as the light source. To obtain a parallel beam with a sufficiently large diameter and uniform intensity distribution, a Keplerian beam expander system was

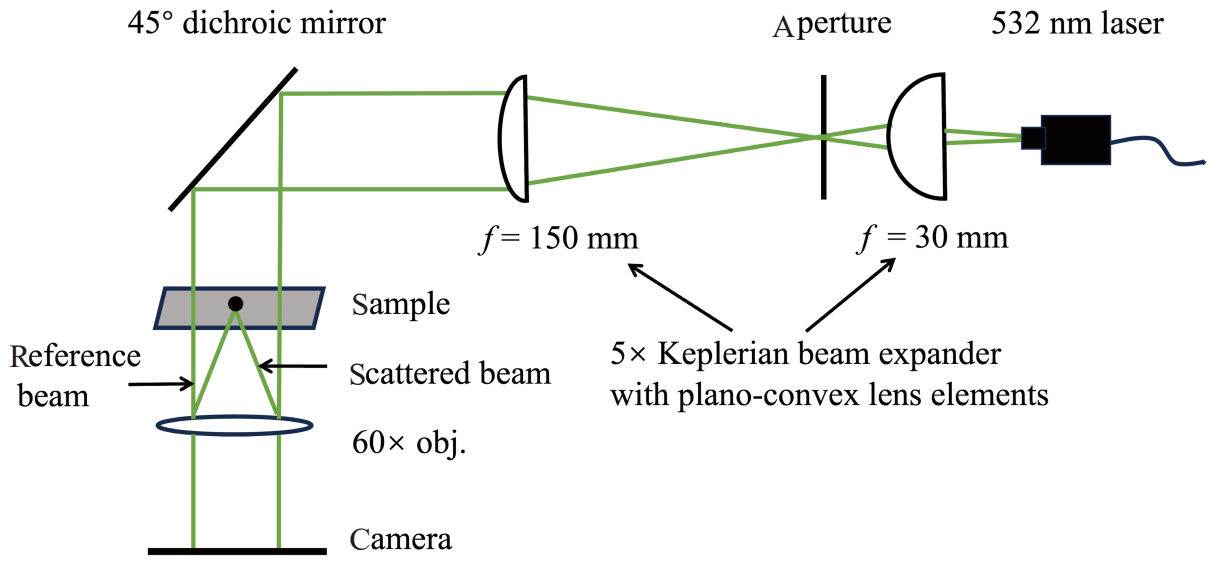

Fig. 1. Schematic of the optical path in the digital holographic microscope.

CSTR: 32290.14.JUSTC-2025-0050
DOI: 10.52396/JUSTC-2025-0050
JUSTC, **2025**, 55(10): 1003

employed, consisting of two plano-convex lenses (focal lengths $f_1 = 30$ mm and $f_2 = 150$ mm, LA1805-A and LA1417-A, Thorlabs), expanding the beam 5-fold, which is sufficient to cover the entire field of view. An aperture diaphragm was used for further spatial filtering. Then a 45°-placed mirror (PF10-03-P01, Thorlabs) was used to introduce the laser into the objective of the microscope (Nikon Ti-E equipped with a 60× water immersion objective (Nikon Plan Apo VC)). The samples were placed on the microscope stage and illuminated with a laser intensity of 10 mW. Holographic images were recorded by a high-speed Hamamatsu CMOS camera mounted on the microscope at a framerate of 100 fps, using 2×2 pixel binning, resulting in images of 1024×1024 pixels per frame.

2.4 Holographic image analysis

In this paper, we aimed to develop a fast and robust algorithm to obtain the 3D position and posture of bacteria. However, existing methods either require expensive computation time and storage or rely on complex algorithms. We optimized the parameter fitting processes to reduce computational time and memory usage through the following procedures, summarized in Table 1.

2.4.1 Image preprocess

Due to the high coherence in digital holographic microscopy, defects in optical elements or contamination in the light path can cause significant background noise in the original hologram images[2], making them unanalyzable, as shown in Fig. 2a. We implemented a simple sliding median filter to extract the background, followed by background subtraction and normalization (setting the average pixel value to 1). This preprocessing procedure yields a clean image of bacterial interference patterns, as shown in Fig. 2b.

2.4.2 Parameters of position and posture estimation

The core algorithm to obtain the parameters is the DDA-LM fitting, but direct utilization of the method may fall into local minimum and global parameter searching is computationally expensive. To reduce time cost and make the algorithm robust, accurate initial parameter estimation is essential. The following methods enable precise initial estimation of bacterial position and orientation, ultimately achieving fast and robust extraction of bacterial 3D location and posture.

Table 1. Hologram processing workflow for bacterial tracking.

Hologram processing
For each of the 200 frames:
Image preprocessing + Initial parameter estimation:
Remove background with a sliding median filter, then normalize.
Locate (X, Y) coordinates via gradient voting.
Identify bacterial axis by analyzing FFT energy distribution differences.
Estimate Z & β via Bayesian scoring using radial minima and directional contrast.
Obtain initial parameter estimates $(X_0, Y_0, Z_0, \beta_0, \varphi_0)$.
DDA-LM fitting:
Optimize the complete parameter set $(X, Y, Z, \beta, \varphi, n, h, d)$ by minimizing the error between experimental holograms and DDA simulations.
End for each frame.

Bacterial center (X, Y) localization. We locate the planar center of each hologram by a gradient-voting strategy. First, we compute the image gradients $\nabla I(x,y)$ with the Sobel operator and retain only pixels whose gradient magnitude exceeds a predefined threshold, thereby isolating the fringe region. For every retained pixel (x,y), we cast votes along the ray in the gradient direction: the pixels receiving votes, regarded as potential centers, obey:

$$(x_{\text{vote}}, y_{\text{vote}}) = (x,y) \pm k \cdot \widehat{\nabla} I(x,y),$$

where $k \in [1, L/2]$ and L denotes the image width. The resulting vote map is smoothed with a Gaussian filter to reduce

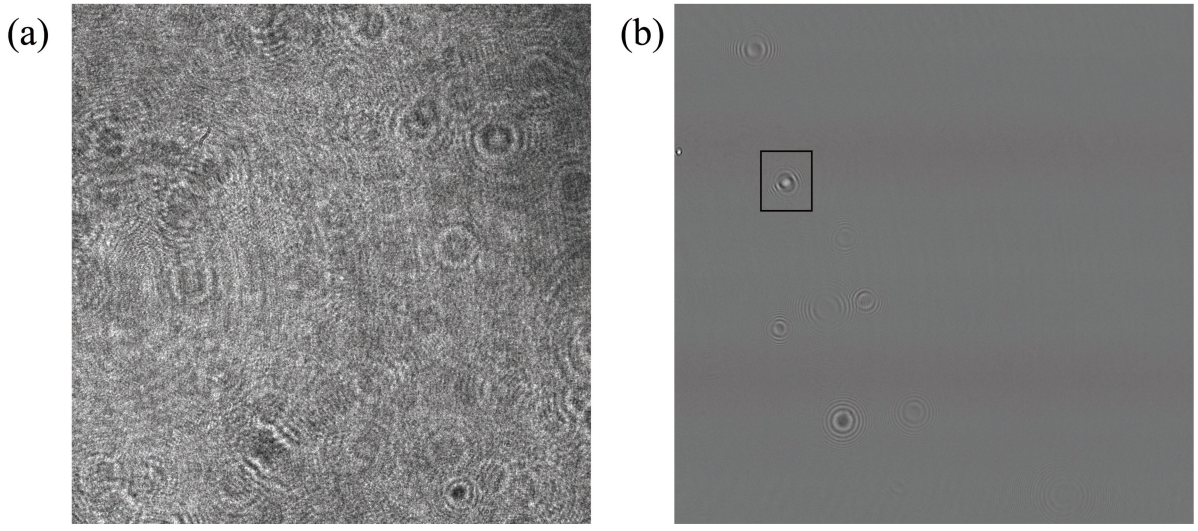

Fig. 2. Comparison of holographic images before and after background processing. (a) Original holographic image exhibiting high background noise and interference speckles. (b) Background-corrected image showing significantly enhanced contrast of interference fringes generated by bacteria (with one bacterium highlighted by a black box), with effective suppression of non-uniform illumination and background noise.

CSTR: 32290.14.JUSTC-2025-0050
DOI: 10.52396/JUSTC-2025-0050
JUSTC, **2025**, 55(10): 1003

spurious peaks. Finally, the global maximum of the smoothed map is taken as the bacterial center. An example is shown in Fig. 3a and b.

Bacterial orientation determination. Fast Fourier transform (FFT) analysis of interference fringes is used to determine the azimuth angle. The high-frequency energy at various angles can be expressed as

$$E(\varphi) = \sum_{k=1}^{N-1} \left| F_{\varphi}(k) \right|^2 ,$$

where $F_{\varphi}(k)$ is the FFT spectrum along φ direction. Then the initial azimuth angle of the bacterial long axis can be determined by°

$$\varphi_{\text{bacteria}} = \text{argmax}_{\varphi} \left(E(\varphi + 90°) - E(\varphi) \right).$$

An example is shown in Fig. 3c and d.

***Z* position and β estimation.** For the strongly coupled parameters of axial position Z and tilt angle β, a joint Bayesian approach is employed for the parameter estimation. Using the previously determined bacterial orientation φ, a series of simulated holograms with varying Z and β values are generated and compared to experimental images. Two critical features are evaluated simultaneously: the radial distribution of fringe minima positions (measured perpendicular to the bacterial long axis) and the directional contrast (measured along and perpendicular to the cell-body axis). A comprehensive score is defined to identify the optimal combination:

$$S(Z, \beta) = w_1 \Delta V(Z, \beta) + w_2 \Delta C(Z, \beta).$$

Here, $S(Z, \beta)$ is the evaluation score, $\Delta V(Z, \beta)$ denotes the weighted difference in fringe minima positions between simulated and experimental holograms, $\Delta C(Z, \beta)$ represents the

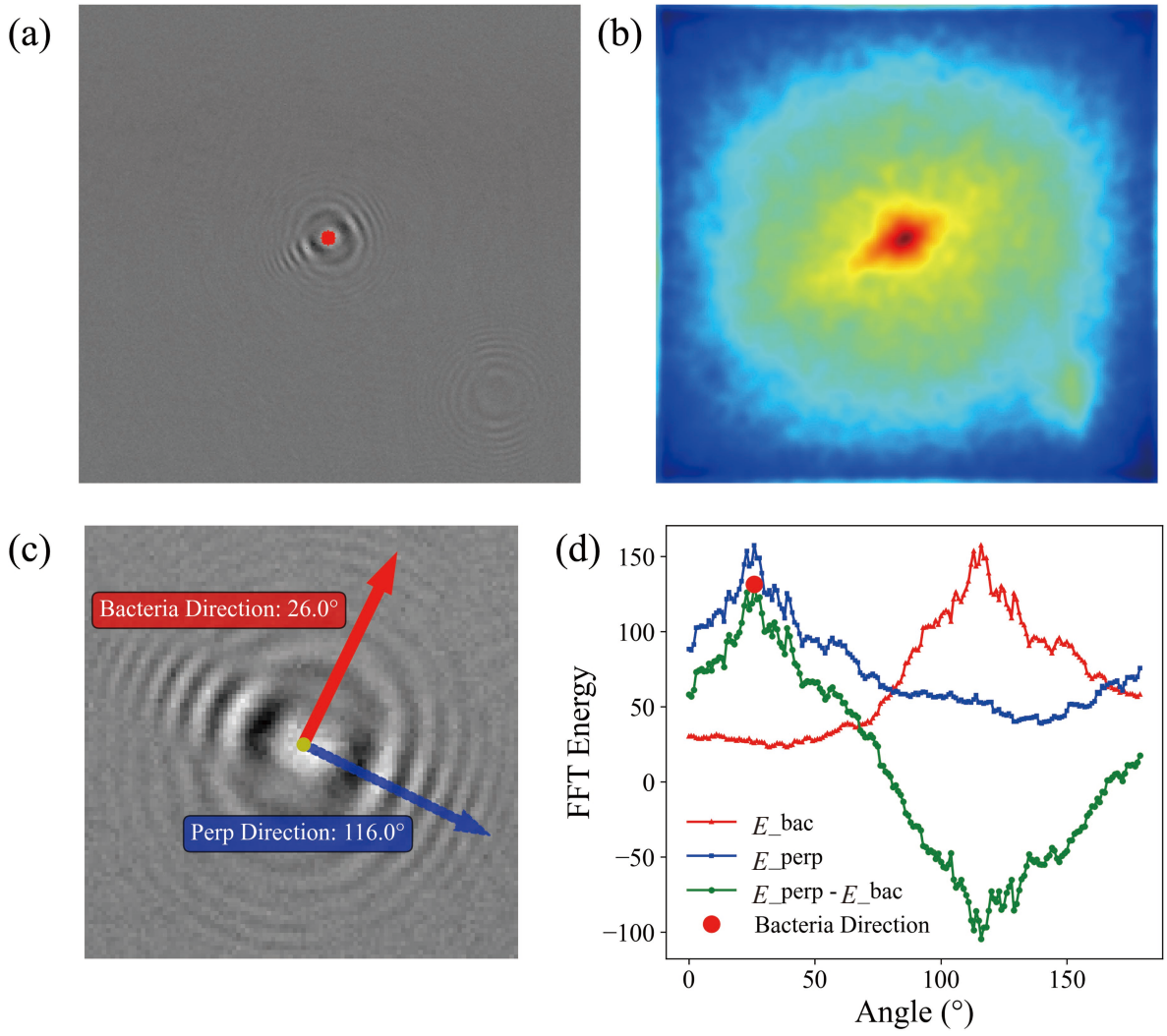

Fig. 3. Determination of bacterial center and orientation. (a, b) Determination of bacterial center position using the voting method. (a) The bacterial center identified by the voting method. (b) The voting hotspot map with the center point corresponding to the maximum voting value. (c, d) Determination of bacterial orientation angle via FFT energy analysis, where (c) illustrates the bacterial main orientation at 26.0° with the corresponding perpendicular direction at 116.0°; (d) presents the FFT energy distribution at different angles, with the red curve (E_{bac}) and blue curve (E_{perp}) represent the energy along the bacterial body axis and perpendicular direction, respectively. The green curve (E_{perp}–E_{bac}) represents the energy difference, where the perpendicular striations are most distinct with highest energy, allowing precise determination of bacterial orientation angle through peak analysis.

CSTR: 32290.14.JUSTC-2025-0050
DOI: 10.52396/JUSTC-2025-0050
JUSTC, **2025**, 55(10): 1003

directional contrast difference, with respective weight coefficients $w_1 = 0.6$ and $w_2 = 0.4$.

DDA-LM fitting. These initial estimates $(X_0, Y_0, Z_0, \beta_0, \varphi_0)$ obtained from the preceding steps serve as priors for the subsequent DDA-LM algorithm.

For calculating the scattering field of non-spherical rod-shaped bacteria, the discrete dipole approximation (DDA)[19] was employed. Bacteria were discretized into multiple small dipoles, each polarizing under the incident field and coupling with neighboring dipoles. After iterative solving, the scattering amplitude and phase of the scatterer in the far field (E_{sca}) are obtained and superimposed with the reference wave to derive the simulated hologram,

$$I_{sim}(x,y) = |E_{ref}(x,y) + E_{sca}(x,y,\boldsymbol{p})|^2,$$

where $\boldsymbol{p} = \{X, Y, Z, \beta, \varphi, n, h, d\}$ comprises the three-dimensional position (X, Y, Z), the inclination and azimuth angles (β, φ), the intracellular refractive index $n = 1.38$[20], and the cell dimensions —length $h = 3$ μm and diameter $d = 1$ μm[21].

Finally, the Levenberg–Marquardt (LM) algorithm from HoloPy[22] minimizes the squared error between experimental and simulated images:

$$S(\boldsymbol{p}) = \sum_{i,j} (\alpha \times I_{exp}(i,j) - I_{sim}(i,j;\boldsymbol{p}))^2,$$

where α represents the overall light intensity scaling factor. To improve accuracy, we employed a customized LM algorithm incorporating noise weighting and utilizing the negative correlation between azimuth angle φ precession frequency and tilt angle β for correction. The improved algorithm iteratively updates parameters $\{X, Y, Z, \beta, \phi, n, h, d\}$, converging rapidly with reasonable initial values. Experiments demonstrate that this "morphological prior + DDA + improved LM" processing pipeline can accurately output bacterial three-dimensional position and orientation within 60 iterations (under 3 min) per frame.

3 Results and discussion

3.1 Error analysis of the algorithm

Fig. 4a–c illustrates a representative fit obtained using the proposed algorithm. To quantify the algorithm's accuracy and robustness, ideal holograms were synthesized at axial positions ranging from 2 μm to 50 μm in 2 μm increments. Each hologram was corrupted with experimental-level noise and fitted 100 times at each depth. The resulting standard deviations of the fitted parameters are plotted in Fig. 4d. We employed this simulation-based approach as a practical substitute for experimental error analysis, since it is not feasible to capture multiple holograms of the same bacterium at precisely controlled positions and orientations in real experiments. While this method does not capture all aspects of experimental uncertainty, it provides a reasonable approximation of the algorithm's intrinsic precision limits.

The axial localisation uncertainty fluctuates with depth but remains within 0.002–0.051 μm. At the primary working plane ($Z = 20$ μm), the uncertainty is approximately 0.018 μm, which is sufficient for three-dimensional tracking experiments. For the orientation parameters, the inclination angle β is recovered with an uncertainty of 12°–17°, whereas the azimuth angle φ is constrained to within 4°–7°. The systematically larger uncertainty in β arises from the reduced sensitivity of the fringe pattern to small tilts when the bacterial long axis is nearly parallel to the solid surface, whereas azimuthal rotations still induce discernible fringe rotation. To further investigate how the inclination angle affects measurement precision, we performed additional simulations with a fixed $Z = 20$ μm while varying β from 10° to 90° (results beyond this range would exhibit symmetrical behavior due to equivalent holographic patterns produced at complementary angles), as shown in Fig. 4e. The results reveal that the uncertainty in Z fluctuates between 0.005 and 0.045 μm. The uncertainty in β increases substantially with the inclination angle, rising from approximately 1° at $\beta = 10°$ to 15° at $\beta = 80°$, while the uncertainty in φ remains relatively stable around 5° across the entire range. This confirms that the algorithm's precision diminishes for bacteria swimming nearly parallel to the surface but remains adequate for tracking through most orientation ranges. Overall, the algorithm maintains reliable spatial and angular precision across the entire 50 μm axial range.

3.2 *E. coli* swimming tracking with hologram

To further test the applicability of the algorithm in real bacteria tracking assays, we performed 3D tracking experiments on *E. coli* swimming near a solid surface. In the experiments, we observed the swimming behavior of the wild-type *E. coli* and recorded holographic images to evaluate the method we presented here. The algorithm successfully captured the swimming dynamics near surface.

3.2.1 Swimming trajectory of *E. coli* near surface

We obtained 22 typical trajectories of *E. coli* using our method and extracted their three-dimensional positions and orientations to analyze their dynamic characteristics. Fig. 5a shows a typical trajectory lasting 2 s, during which the bacterium moved approximately 75.1 μm with an average speed of about 35.5 μm/s. The trajectory forms a clockwise spiral and maintains a relatively stable run phase, consistent with previously reported characteristics of flagellated bacteria swimming near surfaces[2]. The average speed across all bacteria tracked is approximately 30.47 μm/s ± 7.08 μm/s. As shown in Fig. 6a, the speed distribution across all trajectories reveals a peak around 32 μm/s, with most bacteria exhibiting swimming speeds between 25 and 40 μm/s.

The utilization of holographic image technique enabled detailed analysis of bacterial behavior near surface. As shown in Fig. 5a, the angle of the bacterial cell body φ maintains a small offset relative to its direction of motion, manifesting as a precession phenomenon, while overall it rotates in coordination with the trajectory curve. The tilt angle is non-horizontal, showing a slight inclination towards the interface.

3.2.2 Wobbling dynamic of *E. coli*

To analyze the orientation dynamics of the bacteria near surface, we extracted the azimuth angle φ of the bacterial cell body. A typical time series of the directional angle change is

CSTR: 32290.14.JUSTC-2025-0050
DOI: 10.52396/JUSTC-2025-0050
JUSTC, **2025**, 55(10): 1003

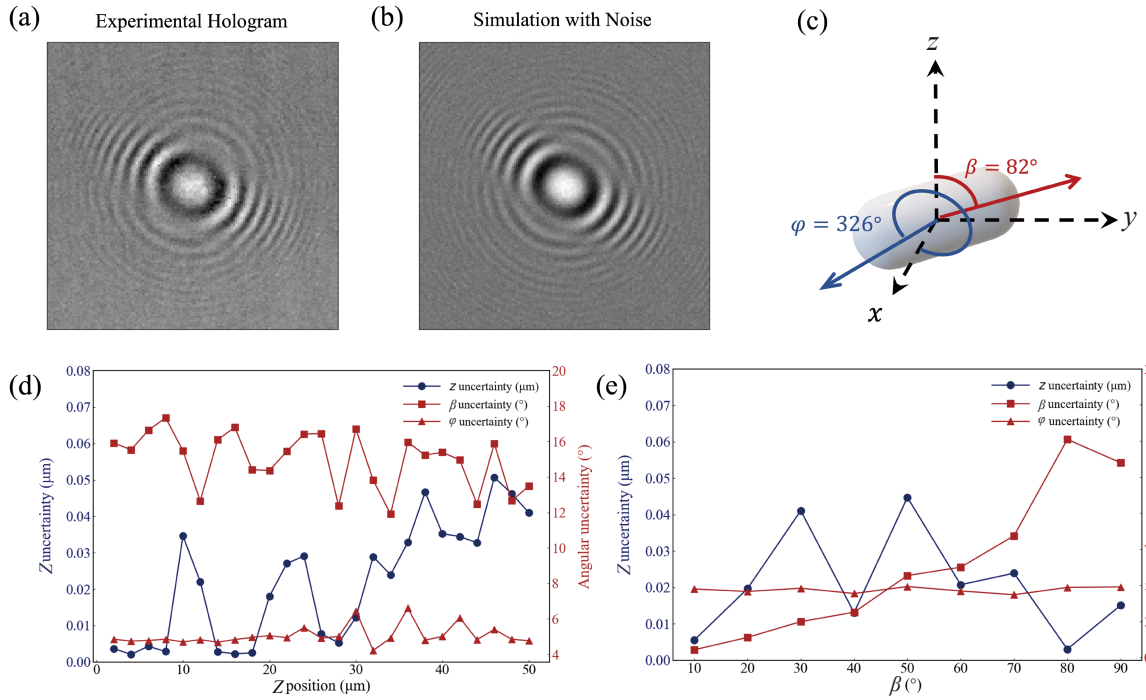

Fig. 4. Fitting accuracy and uncertainty analysis. (a) Background-subtracted experimental hologram. (b) Simulated hologram generated with the parameters obtained from the fit; the fringe morphology closely matches the experimental pattern. (c) Three-dimensional rendering of the fitted bacterium, showing the long axis orientation (inclination β = 82°, azimuth φ = 326°) relative to the laboratory frame. (d) Standard-deviation uncertainties of the fitted parameters as a function of axial position Z (2–50 μm) with fixed β = 90°. The blue circles (left ordinate) indicate the axial localization uncertainty, which ranges from 0.002 to 0.051 μm; at the primary working plane (Z = 20 μm), the uncertainty is 0.018 μm. The red squares and triangles (right ordinate) represent the angular uncertainties: The inclination β is recovered to within 12°–17°, while the azimuth φ remains within 4°–7°. (e) Standard-deviation uncertainties of the fitted parameters as a function of inclination angle β (10°–90°) with fixed Z = 20 μm. The Z uncertainty (blue circles) shows variations between 0.005–0.045 μm. The β uncertainty (red squares) increases significantly with inclination angle, while the φ uncertainty (red triangles) remains relatively stable around 5°. The consistently larger β uncertainty arises because fringe patterns are less sensitive to small tilts when the bacterial long axis is nearly parallel to the solid surface, while changes in azimuth still produce discernible fringe rotation.

shown in Fig. 5b. The trajectory clearly exhibits a clockwise circular curve, consistent with previous observations of bacteria near surfaces. The smoothed azimuth angle $\overline{\varphi}(t)$, calculated using a 20-frames moving average filter, decreases linearly with time, indicating a stable angular change due to hydrodynamic effects. The angular velocity is approximately 2.8045 rad/s. The short-time variation of the body orientation, defined as $\Delta\varphi(t) = |\varphi(t) - \overline{\varphi}(t)|$, is shown in Fig. 5c. $\Delta\varphi(t)$ exhibits periodic oscillations along the time series, characterizing the wobbling dynamics of the cell body. We defined the maximum value of $\Delta\varphi(t)$ within each complete oscillation cycle as the wobble angle φ_w for that cycle. The average wobble angle of the bacterium is obtained by averaging over multiple cycles. The wobble frequency can be inferred from the intervals between peaks in $\Delta\varphi(t)$. In the example shown, the wobble angle of the bacterium is 21.7°, and the wobble frequency is 19.44 Hz. Fig. 5d illustrates the temporal evolution of the bacterial inclination angle β throughout the same trajectory. The inclination angle fluctuates around an average value of 99.7°, indicating that the bacterium maintains a slight tilt toward the surface while swimming.

Through systematic analysis of all 22 trajectories, the results indicate that the average wobble angle is 14.92° ± 5.41°, with a mean wobble frequency of approximately 17.65 Hz ± 5.39 Hz. This frequency is notably lower than the 24 Hz typically observed in free liquid phases[18,23]. The distributions of these parameters are presented in Fig. 6b–d. The wobble frequency distribution (Fig. 6b) shows a clear peak at 15–20 Hz. The inclination angle β exhibits a near-Gaussian distribution centered around 106° (Fig. 6c), indicating that bacteria typically swim with a slight tilt toward the surface. The wobble angle φ_w distribution (Fig. 6d) is primarily concentrated between −25° and 25°, quantifying the extent of directional oscillation during bacterial swimming. This reduction in frequency primarily arises from physical constraints imposed by the surface environment on bacterial movement. First, the solid surface acts as a no-slip boundary, increasing viscous resistance in the fluid medium and producing stronger damping effects on the rotational motion of bacterial flagella. Second, there may be electrostatic or van der Waals interactions between the bacteria and the surface, further restricting the free movement of the bacteria. Finally, the flagella may undergo partial deformation or reorganization near the surface, thereby altering their driving efficiency.

3.2.3 Tilt angle of cell body near surface

As demonstrated in previous study[5], the cell body is not parallel with the surface when swimming near a solid wall. We examined the phenomena in our analysis. We extracted the tilt angles β of *E. coli* cell bodies, finding that the average angle

CSTR: 32290.14.JUSTC-2025-0050
DOI: 10.52396/JUSTC-2025-0050
JUSTC, **2025**, 55(10): 1003

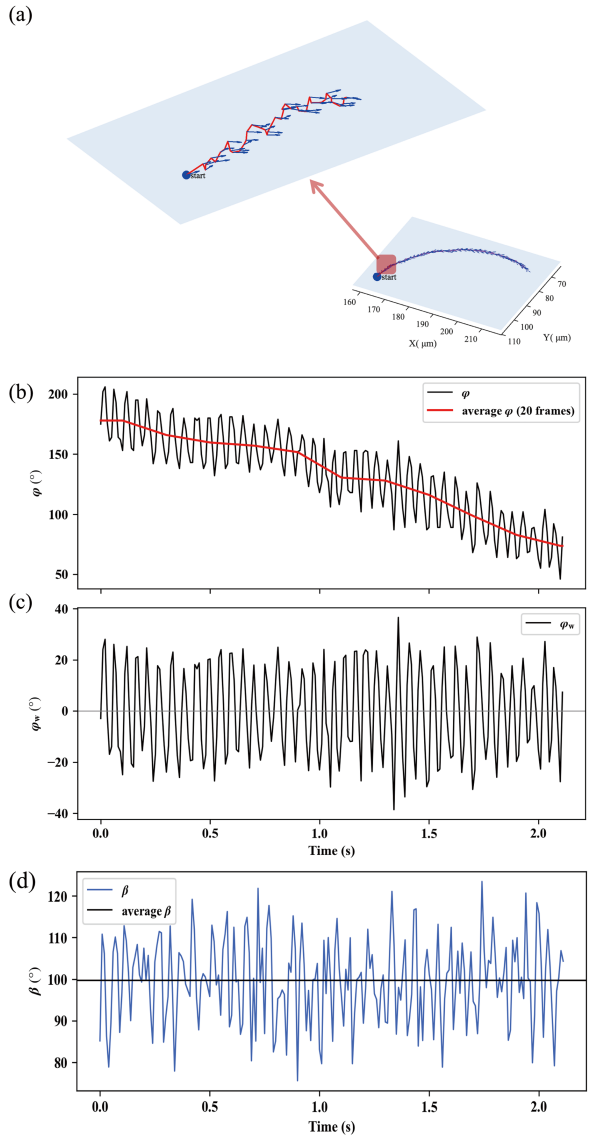

Fig. 5. Swimming trajectory and orientation of *E. coli* near a surface. (a) Three-dimensional trajectory and body orientation of *E. coli* near the solid surface. The main figure shows a detailed view of the first 40 frames (red trajectory), while the inset displays the complete clockwise spiral motion trajectory (pink curve) acquired by digital holographic microscopy. Blue arrow vectors indicate bacterial body orientation at each frame, with the initial position marked as "start". The bottom plane represents the solid surface. The body direction angle φ maintains a small angle relative to the motion trajectory (manifesting as wobble) while simultaneously rotating in coordination with the trajectory curve. The bacterial inclination angle exhibits a non-horizontal state, slightly tilted toward the interface. (b, c) Analysis of direction angle and wobble angle during near-surface swimming of *E. coli*, where (b) shows bacterial direction angle φ over time (black line) and its 20-frame moving average (red line) with an overall decreasing trend accompanied by periodic oscillations due to clockwise swimming (angular velocity ω = 2.8045 rad/s), and (c) displays the wobble angle φ_w calculated as the difference between actual direction angle and average direction angle, reflecting the wobble of the bacterial body during swimming. (d) Time series of the bacterial inclination angle β (blue line), which fluctuates around an average value of 99.7 (black line) throughout the tracked trajectory, demonstrating the cell body's orientation relative to the surface during swimming.

is approximately 105.8°, which corresponds to an angle of 15.8° between the cell body and the surface. The data indicate that bacteria tend to maintain a tilted adhesion state with their heads facing the wall.

To explore the relationship between the wobble amplitude and the tilt angle, we calculated the wobble angle φ_w and the angle of the bacteria relative to the horizontal plane ($\beta - 90°$) for individual bacterium, as shown in Fig. 7. Each symbol in Fig. 7 represents the time-averaged values from a single continuous segment (about 200 frames) of an individual bacterium's trajectory. The data demonstrate a negative correlation between the two parameters, with a correlation coefficient of $r = -0.233$, $p = 0.297$. Although the sample size is relatively small, the result is similar to the observation reported by Bianchi et al.[5]: as the angle between the bacteria and the surface increases and the direct contact of the flagella with the interface decreases, the amplitude of the cell body's wobble becomes smaller. This further validates the applicability of our method and suggests a significant limiting effect of the surface on flagellar rotation and cell body oscillation.

4 Conclusions

The above simulations and experimental studies indicate that the method we implemented here can achieve high-precision tracking of the three-dimensional position and posture of bacteria in near-surface environments. The *Z*-axis positioning reaches sub-micron accuracy, and the angular precision for β and φ sufficiently meets the requirements of bacterial kinematic analysis. Compared with traditional methods, our approach offers several advantages. First, it employs a simple digital holographic microscope to obtain three-dimensional information and the cell body posture of swimming bacteria without the need for fluorescent labeling or staining, thereby avoiding potential impacts of dyes on bacterial physiology. Second, the combination of morphological priors and voting methods significantly improves the convergence efficiency and accuracy of Levenberg–Marquardt (LM) fitting, reducing computational time while achieving high tracking precision. Specifically, our method achieves convergence in approximately 3 min per frame after the initial parameter estimation step, whereas simply using the previous frame's result as the initial guess (a common approach in tracking applications) typically requires 5–10 min to converge or may fail entirely when bacteria undergo significant orientation or position changes between frames. In terms of accuracy, our approach maintains comparable precision to other DDA-based methods while delivering this substantial improvement in processing efficiency. Furthermore, high frame rates enable capturing subtle processes such as bacterial wobble and tilt angle evolution over time, providing deeper insight into the mechanisms of near-surface movement. We validated the method by tracking *E. coli* swimming near a surface and successfully captured the swimming dynamics of the cells.

Using this method, we systematically measured the swimming behavior of *E. coli* near a solid wall. Through the analysis of the trajectories, we obtained data on swimming speed and orientation dynamics. The traces of individual bacteria exhibit clockwise circular curves when near the interface, and the wobble frequency decreased notably. We also observed a negative correlation between the wobble angle and the tilt

CSTR: 32290.14.JUSTC-2025-0050
DOI: 10.52396/JUSTC-2025-0050
JUSTC, **2025**, 55(10): 1003

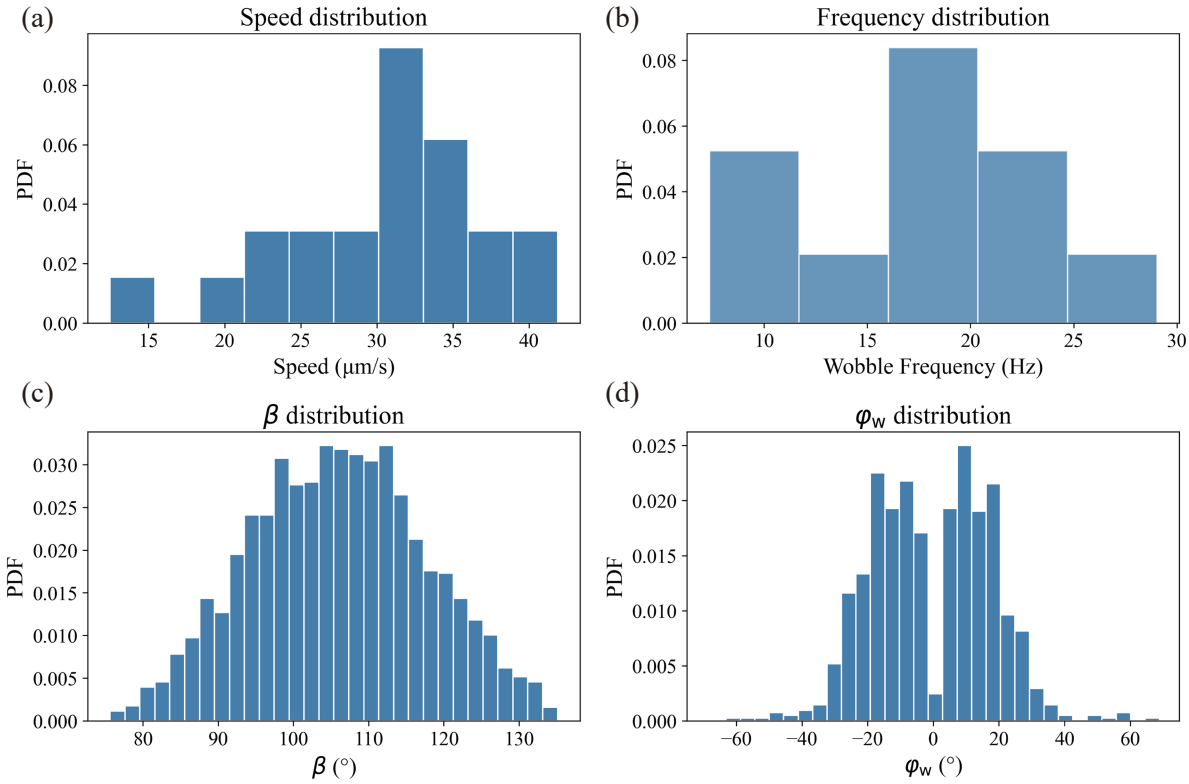

Fig. 6. Statistical distributions of swimming parameters. Statistical distributions of bacterial swimming parameters from 22 trajectories, all *y*-axes represent probability density functions. (a) Distribution of swimming speeds, with a peak around 32 μm/s. (b) Distribution of wobble frequencies, showing the highest probability between 15 and 20 Hz. (c) Distribution of inclination angle β compiled from all frames, exhibiting a near-Gaussian distribution centered around 106°, indicating that bacteria typically swim with a slight tilt toward the surface. (d) Distribution of wobble angle φ_w compiled from all frames, representing the maximum angular deviations from the average swimming direction during wobbling. This distribution spans –50° to 50°, with most values concentrated between –25° and 25°, quantifying the extent of directional oscillation during swimming.

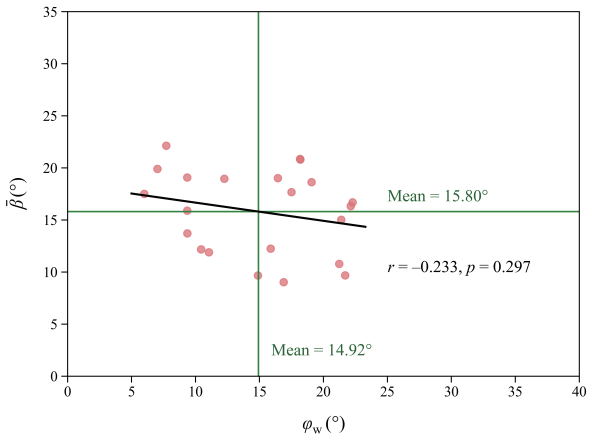

Fig. 7. Relationship between inclination angle and wobble angle. Relationship between bacterial inclination angle (β) relative to the interface and wobble angle (φ_w). Each symbol represents the time-averaged values from a single continuous segment (about 200 frames) of an individual bacterium's trajectory. The horizontal and vertical green lines represent the average bacterial inclination angle relative to the solid surface ($\bar{\beta}$ = 15.80°) and the average wobble angle (φ_w = 14.92°), respectively. The black diagonal line indicates the linear fit between the two parameters. A negative correlation is observed between these parameters ($r = -0.233$, $p = 0.297$).

angle. The observations indicate that the surface environment affects bacterial motility.

The influence of the surface on bacterial movement is primarily realized through two mechanisms: hydrodynamic effects and direct surface–bacteria interactions. From a hydrodynamic perspective, the surface acts as a no-slip boundary condition, altering the flow field distribution around the bacteria. According to the theoretical model by Lauga et al.[1], when a microorganism (such as *E. coli*) approaches a solid surface, the fluid disturbances it generates undergo a "mirror" reflection at the surface, resulting in additional fluid resistance. This effect intensifies sharply as the distance between the bacterium and the surface decreases, especially when the distance is less than the length of the bacterium. Additionally, due to the counter-rotation of the bacterial body and flagella, the asymmetry of the near-surface flow field further causes the bacteria to follow curved trajectories, which explains the observed clockwise movement pattern in this study.

The direct physicochemical interactions between the surface and bacteria also affect motility. According to the DLVO (Derjaguin-Landau-Verwey-Overbeek) theory, there is a combined effect of electrostatic forces and van der Waals forces between the bacteria and the surface[24]. Under physiological conditions, bacterial surfaces are typically negatively charged, leading to electrostatic repulsion with similarly negatively charged solid surfaces (such as glass). However, van der Waals attraction rapidly increases at very close distances.

CSTR: 32290.14.JUSTC-2025-0050
DOI: 10.52396/JUSTC-2025-0050
JUSTC, **2025**, 55(10): 1003

This balance of forces creates a "equilibrium distance" that bacteria tend to maintain, which explains the relatively stable tilt angle distribution observed in this study (average 15.80°). Furthermore, pili on the bacterial surface and surface receptors may form specific or non-specific bindings with the substrate, further affecting their freedom of movement.

We evaluated the impact of bacterial size assumptions on our parameter estimation process. Variations in bacterial length have minimal effect on initial Z-position estimates, as these rely primarily on the vertical light intensity distribution of the cell body, while changes in bacterial width are generally small. However, bacterial size can influence the initial guess for the inclination angle β, since different cell aspect ratios alter the scattering pattern details. To address this, the initial β guess is assigned a relatively broad prior range, and bacterial dimensions (length h and diameter d) are treated as optimizable parameters during the DDA-LM fitting. Tests with varying bacterial lengths (e.g., $h = 2.5$ μm and 3.5 μm, compared to the default 3 μm) showed that although initial guesses varied slightly, final fitted β angle errors typically remained within 5°, demonstrating the algorithm's robustness to physiological size variations. It is important to note that the reported errors reflect fitting uncertainties rather than true measurement errors, which in practice may be larger due to optical aberrations, camera noise, and biological variability.

In summary, the digital holographic microscopy method and algorithm developed in this study provide a powerful and accessible tool for quantitatively analyzing bacterial motility near surfaces with high spatial and temporal resolution. By capturing detailed three-dimensional trajectories and orientation dynamics without invasive labeling, this approach opens new avenues for investigating microbe-surface interactions relevant to biofilm formation, infection processes, and microscale fluid dynamics. Future work may extend this framework to study diverse microorganisms and complex surface environments, further enhancing our understanding of microbial behavior in natural and engineered settings.

Supporting information

The supporting information for this article can be found online at https://doi.org/10.52396/JUSTC-2025-0050. The supporting information includes one example movie of a compressed raw hologram video (Movie S1), and one Python code file for parameter estimation (Initial-parameter-estimation.py).

Acknowledgements

This work was supported by the National Natural Science Foundation of China (11904352).

Conflict of interest

The authors declare that they have no conflict of interest.

Biographies

Xinyi Feng received her master's degree from the School of Physical Sciences, University of Science and Technology of China

Rui He is an Associate Research Fellow at the University of Science and Technology of China (USTC). He received his Ph.D. degree from the School of Physical Sciences, USTC, under the supervision of Prof. Junhua Yuan and Prof. Rongjing Zhang. His research mainly focuses on the bacterial motility and behavior, molecular motor and bacterial chemotaxis in the biological physics field.

References

[1] Lauga E, DiLuzio W R, Whitesides G M, et al. Swimming in circles: Motion of bacteria near solid boundaries. *Biophysical Journal*, **2006**, *90* (2): 400–412.

[2] Molaei M, Barry M, Stocker R, et al. Failed escape: Solid surfaces prevent tumbling of *Escherichia coli*. *Physical Review Letters*, **2014**, *113* (6): 068103.

[3] Berke A P, Turner L, Berg H C, et al. Hydrodynamic attraction of swimming microorganisms by surfaces. *Physical Review Letters*, **2008**, *101* (3): 038102.

[4] Drescher K, Dunkel J, Cisneros L H, et al. Fluid dynamics and noise in bacterial cell-cell and cell-surface scattering. *Proceedings of the National Academy of Sciences*, **2011**, *108* (27): 10940–10945.

[5] Bianchi S, Saglimbeni F, Di Leonardo R. Holographic imaging reveals the mechanism of wall entrapment in swimming bacteria. *Physical Review X*, **2017**, *7* (1): 011010.

[6] Taute K M, Gude S, Tans S J, et al. High-throughput 3D tracking of bacteria on a standard phase contrast microscope. *Nature Communications*, **2015**, *6*: 8776.

[7] Kim M K. Principles and techniques of digital holographic microscopy. *SPIE Reviews*, **2010**, *1* (1): 018005.

[8] Marquet P, Rappaz B, Magistretti P J, et al. Digital holographic microscopy: a noninvasive contrast imaging technique allowing quantitative visualization of living cells with subwavelength axial accuracy. *Optics Letters*, **2005**, *30* (5): 468.

[9] Wilson L G, Carter L M, Reece S E. High-speed holographic microscopy of malaria parasites reveals ambidextrous flagellar waveforms. *Proceedings of the National Academy of Sciences*, **2013**, *110* (47): 18769–18774.

[10] Su T W, Xue L, Ozcan A. High-throughput lensfree 3D tracking of human sperms reveals rare statistics of helical trajectories. *Proceedings of the National Academy of Sciences*, **2012**, *109* (40): 16018–16022.

[11] Xu W, Jericho M H, Meinertzhagen I A, et al. Digital in-line holography for biological applications. *Proceedings of the National Academy of Sciences*, **2001**, *98* (20): 11301–11305.

[12] Garcia-Sucerquia J, Xu W, Jericho S K, et al. Digital in-line holographic microscopy. *Applied Optics*, **2006**, *45* (5): 836–850.

[13] Bishara W, Zhu H, Ozcan A. Holographic opto-fluidic microscopy. *Optics Express*, **2010**, *18* (26): 27499.

[14] Molaei M, Sheng J. Imaging bacterial 3D motion using digital in-line holographic microscopy and correlation-based de-noising algorithm. *Optics Express*, **2014**, *22* (26): 32119.

[15] Jikeli J F, Alvarez L, Friedrich B M, et al. Sperm navigation along helical paths in 3D chemoattractant landscapes. *Nature Communications*, **2015**, *6* (1): 7985.

[16] Kreis T. Handbook of Holographic Interferometry: Optical and Digital Methods. Weinheim, Germany: Wiley-VCH Verlag GmbH & Co. KGaA, **2004**.

[17] Pu Y, Meng H. Intrinsic aberrations due to Mie scattering in particle holography. *Journal of the Optical Society of America A*, **2003**, *20* (10): 1920.

[18] Wang A, Garmann R F, Manoharan V N. Tracking *E. coli* runs and

CSTR: 32290.14.JUSTC-2025-0050
DOI: 10.52396/JUSTC-2025-0050
JUSTC, **2025**, 55(10): 1003

tumbles with scattering solutions and digital holographic microscopy. *Optics Express*, **2016**, *24*(21): 23719–23725.

[19] Yurkin M A, Hoekstra A G. The discrete-dipole-approximation code ADDA: Capabilities and known limitations. *Journal of Quantitative Spectroscopy and Radiative Transfer*, **2011**, *112* (13): 2234–2247.

[20] Nadeau J L, Cho Y B, Lindensmith C A. Use of dyes to increase phase contrast for biological holographic microscopy. *Optics Letters*, **2015**, *40* (17): 4114.

[21] Berg H C. *E. coli* in Motion. New York, NY, USA: Springer, **2004**.

[22] Barkley S, Dimiduk T G, Fung J, et al. Holographic microscopy with Python and HoloPy. *Computing in Science & Engineering*, **2019**, *22* (5): 72–82.

[23] Darnton N C, Turner L, Rojevsky S, et al. On torque and tumbling in swimming *Escherichia coli*. *Journal of Bacteriology*, **2007**, *189* (5): 1756–1764.

[24] Busscher H J, van der Mei H C. Microbial adhesion in flow displacement systems. *Clinical Microbiology Reviews*, **2006**, *19* (1): 127–141.

CSTR: 32290.14.JUSTC-2025-0050
DOI: 10.52396/JUSTC-2025-0050
JUSTC, **2025**, 55(10): 1003